Crystallographic Studies on the Role of the C-Terminal Segment of Human Angiogenin in Defining Enzymatic Potency[†,‡]

Demetres D. Leonidas,[§,||] Robert Shapiro,[⊥,@] Gowtham V. Subbarao,[§,▽] Aniello Russo,[⊥,#] and K. Ravi Acharya*[,§]

Department of Biology and Biochemistry, University of Bath, Claverton Down, Bath BA2 7AY, U.K., and Center for Biochemical and Biophysical Sciences and Medicine and Department of Pathology, Harvard Medical School, Boston, Massachusetts 02115

Received September 12, 2001; Revised Manuscript Received November 13, 2001

ABSTRACT: Human angiogenin (Ang) is an RNase in the pancreatic RNase superfamily that induces angiogenesis. Its catalytic activity is comparatively weak, but nonetheless critical for biological activity. The crystal structure of Ang has shown that enzymatic potency is attenuated in part by the obstructive positioning of Gln117 within the B_1 pyrimidine binding pocket, and that the C-terminal segment of residues 117−123 must reorient for Ang to bind and cleave RNA. The native closed conformation appears to be stabilized by Gln117−Thr44 and Asp116−Ser118 hydrogen bonds, as well as hydrophobic packing of Ile119 and Phe120. Consistent with this view, Q117G, D116H, and I119A/F120A variants are 4−30-fold more active than Ang. Here we have determined crystal structures for these variants to examine the structural basis for the activity increases. In all three cases, the C-terminal segment remains obstructive, demonstrating that none of the residues that has been replaced is essential for maintaining the closed conformation. The Q117G structure shows no changes other than the loss of the side chain of residue 117, whereas those of D116H and I119A/F120A reveal C-terminal perturbations beyond the replacement site, suggesting that the native closed conformation has been destabilized. Thus, the interactions of Gln117 seem to be less important than those of residues 116, 119, and 120 for stabilization. In D116H, His116 does not replicate either of the hydrogen bonds of Asp116 with Ser118 and instead forms a water-mediated interaction with catalytic residue His114; residues 117−121 deviate significantly from their positions in Ang. In I119A/F120A, the segment of residues 117−123 has become highly mobile and all of the interactions thought to position Gln117 have been weakened or lost; the space occupied by Phe120 in Ang is partially filled by Arg101, which has moved several angstroms. A crystal structure was also determined for the deletion mutant des(121−123), which has 10-fold reduced activity toward large substrates. The structure is consistent with the earlier proposal that residues 121−123 form part of a peripheral substrate binding subsite, but also raises the possibility that changes in the position of another residue, Lys82, might be responsible for the decreased activity of this variant.

Human angiogenin (Ang),[1] a monomeric protein of 123 amino acids, is a ribonucleolytic enzyme in the pyrimidine-specific pancreatic RNase superfamily that induces formation of new blood vessels in vivo (for recent reviews, see refs *3* and *4*). It was first isolated from medium conditioned by human colon adenocarcinoma cells (*5*), and has since been demonstrated to play a critical role in the establishment of a wide range of human tumor xenografts in athymic mice (*6*−*9*), most likely by contributing to tumor angiogenesis. Moreover, Ang expression is elevated in numerous types of human cancers, and in many instances, increased Ang levels have been shown to be associated with cancer aggressiveness and/or progression (*10*−*18*). These findings identify Ang as an attractive target for anticancer therapy.

The precise molecular mechanism by which Ang induces neovascularization has not been determined. However, mutational studies have established that the ribonucleolytic active center of the protein is a key participant. Individual replacements of catalytic and substrate-binding residues simultaneously attenuate both enzymatic and angiogenic activities (*19*−*21*); crystal structures determined for two of the catalytic site variants reveal that there are no significant changes beyond the mutation sites (*22*). Thus, detailed knowledge

[†] This work was supported by The Cancer Research Campaign (CRC) (U.K.) (Project Grant SP2354/0102 to K.R.A.), the Medical Research Council (U.K.) (Programme Grant 9540039 to K.R.A.), Wellcome Trust Biomedical Research Collaboration Grant 044107/Z/95/Z (K.R.A. and R.S.), the National Institutes of Health (Grants HL52096 and CA88738 to R.S.), the Endowment for Research in Human Biology, Inc., Boston (R.S. and A.R.), a Royal Society-Leverhulme Trust (U.K.) Senior Research Fellowship to K.R.A., and a University of Bath postgraduate bursary to G.V.S.

[‡] The atomic coordinates of the four angiogenin variants have been deposited with the RCSB Protein Data Bank [entries 1K58, 1K59, 1K5A, and 1K5B for D116H, Q117G, I119A/F120A, and des(121−123) variants, respectively].

* To whom correspondence should be addressed. Telephone: 44-1225-826 238. Fax: 44-1225-826 779. E-mail: K.R.Acharya@bath.ac.uk.

[§] University of Bath.

[||] Present address: Institute of Biological Research and Biotechnology, The National Hellenic Research Foundation, 48 Vas. Constantinou Ave., Athens 116 35, Greece.

[⊥] Center for Biochemical and Biophysical Sciences and Medicine, Harvard Medical School.

[@] Department of Pathology, Harvard Medical School.

[▽] Present address: Department of Molecular and Experimental Medicine, The Scripps Research Institute, 10550 N. Torrey Pines Rd., La Jolla, CA 92037.

[#] Present address: Department of Life Sciences, Second University of Naples, Via Vivaldi 43, 81100 Caserta, Italy.

[1] Abbreviations: Ang, angiogenin; Pyr, pyroglutamic acid; rms, root-mean-square.

10.1021/bi015768q CCC: $22.00
Published on Web 01/30/2002

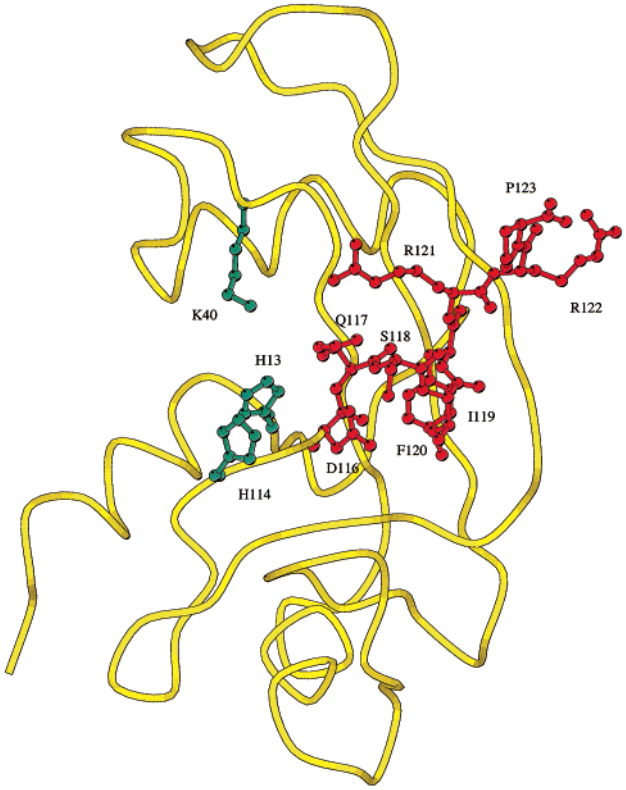

FIGURE 1: Representation of the Ang structure showing the C-terminal segment (residues 116−123) in red and the side chains of the three catalytic residues (His13, Lys40, and His114) in cyan.

of the enzymatic properties of Ang and their structural basis is essential for understanding the biological function of this protein, and may provide a route to the development of Ang antagonists for clinical use.

The most striking aspect of the ribonucleolytic activity of Ang is its weakness with standard RNase substrates; e.g., Ang cleaves dinucleotides and tRNA 10^5−10^6 times less rapidly than does RNase A (*23*−*26*). The reason for this low activity is not apparent from the amino acid sequence (*27*), which shows all three of the catalytic residues of RNase A (His12, Lys41, and His119) are conserved in Ang (as His13, Lys40, and His114, respectively) along with many important substrate binding components. However, the crystal and solution structures of human (*22*, *28*, *29*) and bovine Ang (*30*, *31*), together with the results of extensive mutational studies (*26*, *32*−*35*), have revealed several unique features of the protein that contribute to the attenuation of enzymatic potency (discussed in ref *22*). Chief among these is the obstructive positioning of Gln117 (Glu118 in bovine Ang) within the site that corresponds to the open pyrimidine binding pocket of RNase A. Indeed, this blockage is the structural "trademark" of Ang. Modeling indicates that binding and cleavage of RNA substrates cannot occur unless Ang undergoes a conformational change to alleviate the occlusion (*34*), and that movement of the side chain of residue 117 alone would not suffice.

The inactive structure seen in native human Ang crystals appears to be maintained by several interactions within the C-terminal segment containing Gln117, and others that link this segment with adjacent elements (Figures 1 and 2). Gln117 itself forms two hydrogen bonds with Thr44, and the residues flanking this glutamine, Asp116 and Ser118, are linked by two hydrogen bonds. The orientation of Gln117 seems to be dictated further by the secondary structure of the segment 117−121, a 3_{10} helix in which main chain hydrogen bonds connect Gln117 with Phe120, and Ser118 with Arg121. Finally, hydrophobic packing of the side chains of Ile119 and Phe120 may play a part in fixing the position of the helix and the direction in which it travels.

The roles of the residues in the C-terminal segment 116−123 have been examined by mutagenesis. Replacements of Gln117 with Gly and Ala increase enzymatic activity toward tRNA by 30- and 18-fold, respectively, consistent with the deleterious location of the side chain of residue 117 in the three-dimensional structure (*34*). Substitutions of Asp116 produce increases in activity toward RNA of up to 18-fold (D116H) (*32*, *36*). Mutation of Ser118 to Ala enhances activity by 7-fold (*35*), and simultaneous replacement of Ile119 and Phe120 with Ala results in a 4-fold activation (*33*). Deletion of the three C-terminal amino acids [generating des(121−123) Ang] has only a small effect on cleavage of dinucleotides, but diminishes activity toward tRNA by 10-fold, suggesting that these residues make a positive contribution to cleavage of large substrates (*33*).

In the study presented here, we have investigated the structural basis for the altered functional properties of the D116H, Q117G, I119A/F120A, and des(121−123) Ang variants (Table 1) by X-ray crystallography. In the crystal structures of the first three superactive proteins, the conformation of the C-terminal segment remains obstructive, indicating that none of the replacements by itself is sufficient to trigger the reorientation required to provide access to the pyrimidine binding site. However, the closed conformation appears to have been destabilized in D116H and I119A/F120A. The des(121−123) structure is consistent with the view that residues 121−123 form part of a peripheral subsite for binding polynucleotide substrates, but also raises an alternative possibility.

EXPERIMENTAL PROCEDURES

Preparation and Crystallization of Ang Variants. Variants, all in the natural pyroglutamic acid-1 (Pyr1) form, were produced in *Escherichia coli* with the expression plasmid pAng3 (*32*−*34*, *37*). Crystals were grown at 16 °C using the vapor diffusion technique, by equilibrating a 1:1 mixture of protein (20 mg/mL in water) and reservoir buffer against the reservoir buffer. With Q117G and des(121−123), this buffer was the same as that used for native Ang [0.2 M sodium potassium tartrate and 20 mM sodium citrate (pH 5.2) with 10−15% (w/v) PEG 6000 (*22*, *38*)]. The reservoir buffer for D116H crystallization was 0.1 M sodium citrate (pH 5.6), 20% (v/v) 2-propanol, and 20% (w/v) PEG 4000, and that for I119A/F120A was 0.2 M ammonium acetate and 0.1 M sodium citrate (pH 5.6) with 30% (w/v) PEG 4000. D116H crystallized in the $P4_12_12$ space group, whereas the other variants, like wild-type Ang, crystallized in the $P2_12_12$ space group. Crystallographic details are listed in Table 2.

Data Processing and Reduction. Diffraction data were collected for all four Ang variants on a Siemens area detector mounted on a Siemens rotating anode X-ray source with Cu Kα radiation operating at 45 kV and 80 mA. Additional data

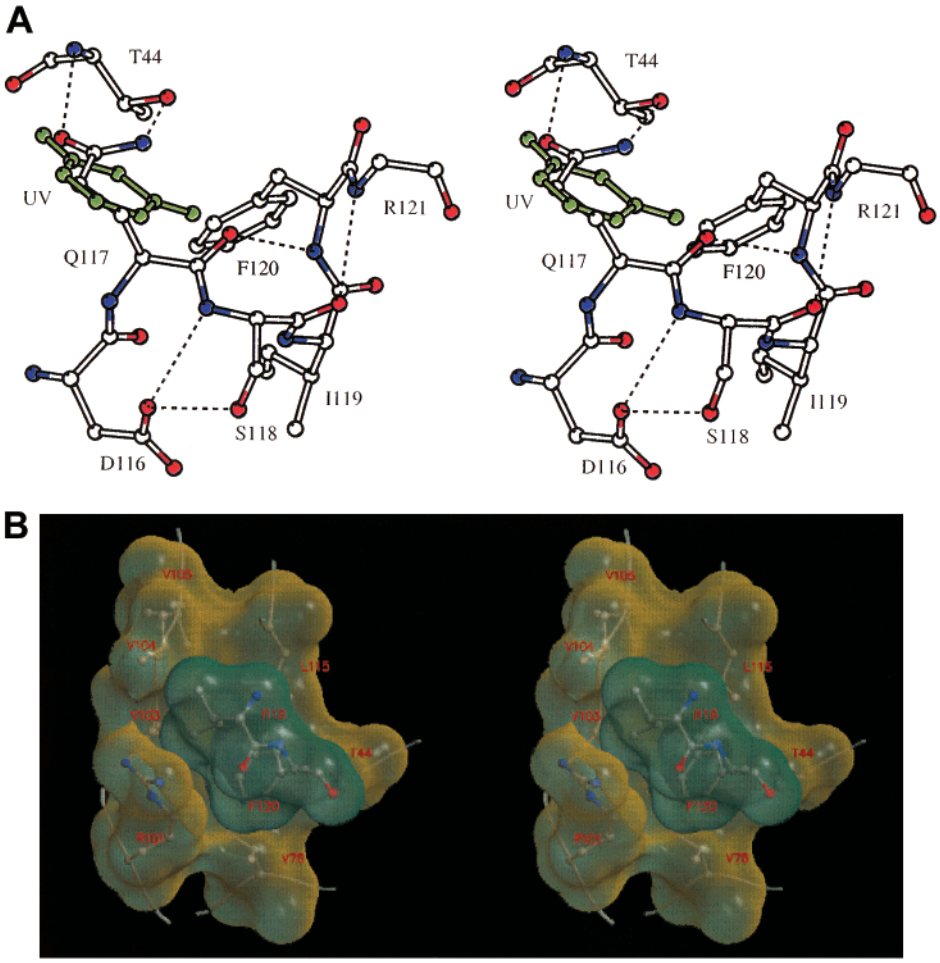

FIGURE 2: Stereoviews of the interactions of the C-terminal segment of wild-type Ang. Panel A shows the hydrogen bonds (dashed lines) of residues 116−121, with residue atoms in standard colors; in addition, the uracil moiety of uridine vanadate (UV, green), taken from the structure of the UV−RNase A complex (*65*) superimposed onto that of Ang, is shown to highlight the blockage of the B_1 site by Gln117. The side chain of Arg121 has been omitted for clarity. Panel B shows the hydrophobic contacts of Ile119 and Phe120. van der Waals surfaces of Ile119 and Phe120 are in cyan, and those of Thr44, Val78, Arg101, Val103, Val104, Val105, and Leu115 are in yellow. This figure was generated with the program GRASP (*72*).

Table 1: Enzymatic Activities of Angiogenin Variants Relative to That of Angiogenin[a]

enzyme	tRNA	CpA	UpA	enzyme	tRNA	CpA	UpA
wild-type	1	1.0	1.0	I119A/F120A	4	3.3	3.2
D116H	18	3.7	3.0	des(121−123)	0.1	0.7	0.5
Q117G	30	25	22				

[a] Relative activities that are listed are based on data from refs *32* (D116H), *34* (Q117G), and *33* [I119A/F120A and des(121−123)]. Activities toward CpA and UpA represent k_{cat}/K_m values taken from the first-order reaction measured at a substrate concentration well below K_m. The activities toward tRNA are initial reaction rates in an assay that assesses production of perchloric acid-soluble RNA fragments (*24*); the substrate concentration that was used was similar to the apparent K_m value.

Table 2: Data Collection Statistics

	D116H	Q117G	I119A/F120A	des(121−123)
space group	$P4_12_12$	$P2_12_12$	$P2_12_12$	$P2_12_12$
unit cell				
a (Å)	35.98	86.65	88.12	86.45
b (Å)	35.98	37.63	41.16	40.41
c (Å)	199.93	38.78	33.66	32.98
resolution (Å)	30.0−2.7	40.0−1.8	35.0−2.3	30.0−1.8
no. of reflections measured	13508	94895	24206	38216
R_{sym} [a] (%)	7.3	4.4	8.7	7.3
no. of unique reflections	3781	11982	5235	10158
completeness (outermost shell)[b] (%)	92.3 (52.4)	98.3 (96.3)	88.0 (32.0)	92.3 (90.0)
$I/\sigma(I)$ (outermost shell)[b]	13.3	7.8	15.5	11.7

[a] $R_{sym} = \sum_h\sum_i|I(h) - I_i(h)|/\sum_h\sum_i I_i(h)$, where $I_i(h)$ and $I(h)$ are the *i*th and mean measurements of the intensity of reflection *h*, respectively. [b] Outermost shell: 2.8−2.7 (D116H), 1.9−1.8 [Q117G and des(121−123)], and 2.4−2.3 (I119A/F120A).

to high resolution (1.8 Å) for variant Q117G and des(121−123) were collected on station PX 9.5 (λ = 0.8 Å) of the Synchrotron Radiation Source (Daresbury, U.K.) using a 30 cm diameter MAR research image plate. The XDS program (*39*) was used for raw area detector data processing and reduction. Raw data images from the synchrotron source were indexed, integrated, and corrected for Lorentz and polarization effects using the program DENZO (*40*). All data were scaled and merged using the program SCALEPACK (*40*). Intensity measurements from the area detector and synchrotron were merged and scaled by the program SCALA (*41*). Intensities were truncated to amplitudes by the TRUNCATE program (*42*). Details of the data processing statistics are presented in Table 2.

Table 3: Refinement Statistics

	D116H	Q117G	I119A/F120A	des(121−123)
resolution (Å)	30.0−2.7	20.0−1.8	20.0−2.3	20.0−1.8
R_{cryst} [a] (%)	19.1	19.6	19.3	20.6
R_{free} [b] (%)	36.0	24.1	28.1	27.5
no. of reflections	3779	11958	5222	9945
no. of protein atoms	994	987	938	967
no. of solvent molecules	31	70	41	57
no. of citrate molecules	−	1	−	1
rms deviations from ideality				
bond lengths (Å)	0.012	0.010	0.010	0.009
bond angles (deg)	1.7	1.6	1.5	1.8
dihedrals (deg)	29.0	27.0	27.9	27.5
impropers (deg)	0.9	0.8	0.8	0.8
average *B* factor (Å^2)				
main chain atoms	22.2	23.3	29.7	26.2
side chain atoms	24.4	29.0	33.5	31.0
all protein atoms	23.3	26.1	31.6	28.6
solvent atoms	31.7	40.9	44.8	42.5

[a] $R_{cryst} = \sum_h|F_o - F_c|/\sum_h F_o$, where F_o and F_c are the observed and calculated structure factor amplitudes of reflection *h*, respectively. [b] R_{free} is equal to R_{cryst} for a randomly selected 5% subset of reflections not used in the refinement (*48*).

Phasing and Refinement. The structures of all four Ang variants were determined by the method of molecular replacement using the program AMoRe (*43*) with the coordinates of human Ang (Pyr1 form) at 1.8 Å resolution (*22*) as a search model. The output model from AMoRe for every Ang variant was subjected to rigid-body refinement with X-PLOR 3.851 (*44*). Alternating cycles of manual building, conventional positional refinement, and the simulated annealing method as implemented in X-PLOR improved each model. Rebuilding was initially performed at 3.0 Å resolution using program O version 5.10.3 (*45*). Extension of the refinement from 3.0 Å to higher resolution was performed in 0.1 Å resolution steps, and the quality of each model was monitored using sigmaA-weighted $2|F_o| - |F_c|\phi_{calc}$ maps calculated using the program SIGMAA (*46*) improved by solvent flattening, histogram matching, and density modification using the program DM (*47*). The behavior of the R_{free} (*48*) value was also monitored throughout the refinement. During the final stages of refinement, water molecules were inserted into the models only if there were peaks in the $|F_o| - |F_c|$ electron density maps with heights greater than 3σ and they were at hydrogen bond forming distances from appropriate atoms. The $2|F_o| - |F_c|\phi_{calc}$ maps were also used to check the consistency in peaks. Water molecules with a temperature factor of >60 Å^2 were excluded from subsequent refinement steps. At the final stages of refinement, all data from 20.0 Å resolution were included and solvent correction was applied as implemented in X-PLOR 3.851 (*49*) (Table 3).

The program PROCHECK (*50*) was used to assess the quality of the final structures. Analysis of the Ramachandran ($\varphi-\psi$) plots for the four structures showed that all residues lie in the allowed regions. Structural superimpositions were performed using the program SHP (*51*), and figures were drawn with Molscript (*52*) as modified by R. Esnouf (*53*).

RESULTS AND DISCUSSION

Overall Structures of D116H, Q117G, I119A/F120A, and des(121−123) Ang Variants. In general, the structures of all four variants are well-defined in the electron density map except for the N- and C-termini and some side chains on the surface, as in the native structure (*22*). There is no density for residues 1 and 2 in I119A/F120A even at 0.6σ; in the other variants, these residues had some density at 0.8σ and were modeled. Residues 122 and 123 are disordered in D116H and Q117G. There is no density for residues 121−123 in the I119A/F120A structure and only weak density for 119 and 120 at 0.8σ. In contrast, the C-terminal segment of des(121−123) is well-ordered through to the end. Outside of the N- and C-terminal regions, there is no density for all or part of the following side chains: Lys17 (in all structures but D116H), Gln19 [D116H and des(121−123)], Arg24 (all but Q117G), Arg31 (Q117G and I119A/F120A), Arg32 (Q117G), Arg51 (D116H and Q117G), Lys54 (Q117G), Lys60 (all), Arg66 (all), Glu67 (D116H and I119A/F120A), Lys82 [all but des(121−123)], and Arg95 (all). There are 31, 70, 41, and 59 water molecules in the structures of D116H, Q117G, I119A/F120A, and des(121−123), respectively. The structures of Q117G and des(121−123) each contain one citrate molecule from the crystallization buffer, bound outside the active site region.

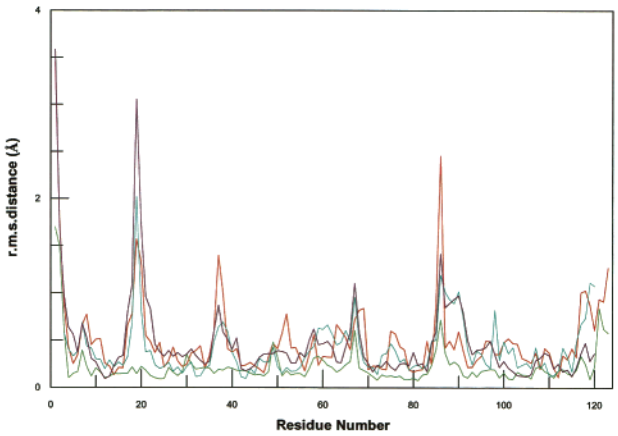

FIGURE 3: Diagram showing the rms distances of the main chain atoms of wild-type Ang from those of the D116H (red), Q117G (green), I119A/F120A (blue), and des(121−123) (purple) variants in the superimposed structures.

If the disordered residues at the termini are excluded, the structures of D116H, Q117G, I119A/F120A, and des(121−123) Ang superimpose with that of native Ang at 1.8 Å resolution (*22*) with rms deviations of 0.50, 0.20, 0.43, and 0.52 Å, respectively, for 119 (D116H and Q117G) or 118 [I119A/F120A and des(121−123)] equivalent C_α atoms. Apart from the C-terminal region, only surface loop residues show ≥1 Å deviations in the positions of main chain atoms (Figure 3): Gln19 (all structures except Q117G), Ser37 (D116H), Glu67 [des(121−123)], and the loop of residues 85−92 (all but Q117G). The orientations of side chains are largely similar in the variant and wild-type structures, except for several surface residues and amino acids in the vicinity of the mutation sites.

Structure of D116H Ang. The role of Asp116 in Ang was first investigated by site-specific mutagenesis prior to the determination of the Ang crystal structure. This aspartate was considered to be of interest because it is analogous to Asp121 of RNase A, a residue that is conserved throughout the pancreatic RNases (*54*) and had been shown to make a significant contribution to activity in a semisynthetic form

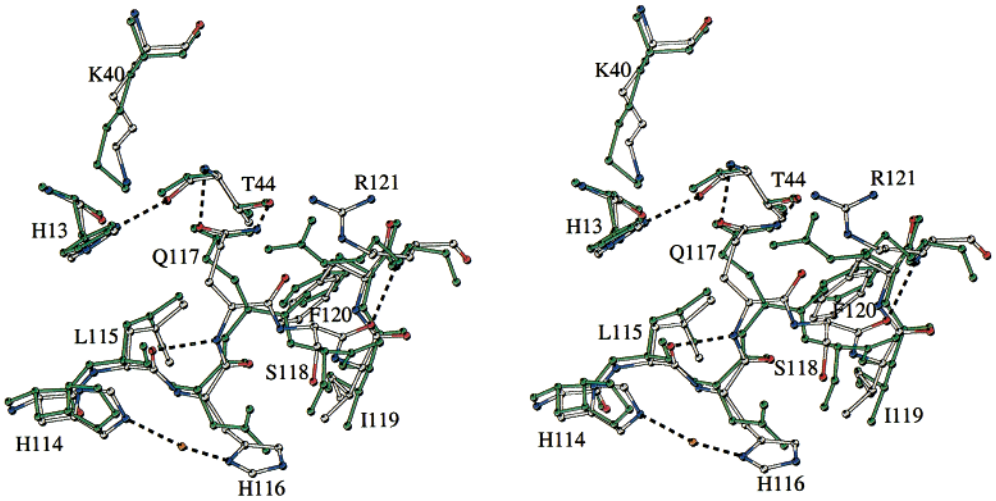

FIGURE 4: Stereoview of the superimposed structures of wild-type Ang (green) and D116H (standard coloring scheme) showing the C-terminal segment of residues 114−121 plus Thr44 and catalytic residues His13 and Lys40. A water molecule in the D116H structure is shown in orange. Hydrogen bonds in D116H are represented as dashed lines. Residue labels refer to the variant.

of the enzyme [RNase(1−118)·(111−124) (*55*)]. Crystal structures of RNase A and its nucleotide complexes (*56*−*58*) had revealed a hydrogen bond of the Asp carboxylate with Nδ1 of His119 that was postulated to help orient His119 for catalysis [as subsequently confirmed by functional and structural analysis of D116N and D116A variants, which were 3−160-fold less active than the wild-type enzyme (*59*)].

Contrary to expectations based on RNase A, replacement of Asp116 in Ang demonstrated that this amino acid acts to suppress enzymatic activity. Substitutions by His, Ser, Ala, Glu, Asn, Lys, and Val increased the effectiveness of Ang toward tRNA by factors of 18, 16, 15, 9, 8, 4, and 2, respectively (*32*, *36*). These findings were mysterious until the advent of the Ang crystal structure (*28*), which showed the side chain of Asp116 is oriented quite differently from that of Asp121 in RNase A. Rather than interacting with catalytic residue His114 (the analogue of His119 in RNase A), Asp116 swings away from it and forms two hydrogen bonds with Ser118 (Oδ1 to Oγ and N) (Figure 2A) that appear to contribute to the obstructive positioning of Gln117 within the B_1 pyrimidine binding site.[2] This suggested that the activity increases associated with replacements of Asp116 might be consequences of eliminating one or both of the hydrogen bonds between residues 116 and 118 (Nδ1 of His is structurally analogous to one of the δ oxygens of Asp, and the Asp116 to His replacement could potentially retain one of the two hydrogen bonds with Ser118).

The crystal structure of the D116H variant, determined at 2.7 Å resolution, reveals that in fact His116 does not form any hydrogen bond with Ser118 (Figure 4 and Table 4). The two imidazole nitrogens of His116 are 4.9 and 3.8 Å from Oγ of Ser118, and even farther from the backbone N of residue 118. Interchanging His116 atoms Cδ2 and Nϵ2 with Nδ1 and Cϵ1, respectively, does not diminish these distances significantly (the crystal structure cannot distinguish between the two possible His rotamers). The increased distance between residues 116 and 118 in D116H reflects movements of both residues. Nδ1 and Nϵ2 of His116 are each ∼2 Å from Oδ1 of Asp116 in the superimposed wild-type and variant structures; this shift moves the side chain of residue 116 closer to the imidazole of His114, with which it forms a water-mediated hydrogen bond (Nδ1−Nϵ2). Oγ and N of Ser118 in D116H are 1.9 and 0.9 Å, respectively, from their locations in wild-type Ang. The movement of the main chain of residue 118 is part of a more general perturbation of the C-terminal segment starting at position 117. The rms deviations for the positions of residues 117−121 in the wild-type and D116H structures are 0.90 Å (main chain only) and 1.15 Å (all atoms), and residues 117−121 in D116H no longer form a 3_{10} helix (Table 4). Despite this partial reorientation, the side chains of Ile119 and Phe120 maintain their low solvent accessibility.

Importantly, the putative B_1 site remains blocked in D116H; i.e., elimination of the two hydrogen bonds between residues 116 and 118 present in wild-type Ang is not sufficient to remove Gln117 from its obstructive position (Figure 4). The side chain amide of Gln117 in D116H superimposes well with that in Ang and forms the same two hydrogen bonds with Thr44 (Table 4), despite a ∼1 Å shift in the position of C_α.

All of the residues thought to interact directly with the core dinucleotide of RNA substrates are oriented similarly in the D116H and wild-type structures. These include His13, Lys40, His114, Gln12, and Leu115 (N) at the P_1 subsite (*60*); Thr44, which plays a major role in defining pyrimidine specificity; and Glu108, which has a minor role in binding purines at the B_2 subsite (*21*). Two functionally important residues outside this central region, Arg5 and His8, deviate appreciably in the two structures. Arg5 forms part of the P_2 subsite (*61*); its guanidino group in D116H is positioned 4−5 Å away from that in Ang and makes a hydrogen bond with the Glu108 carboxylate that is not present in Ang. However, the significance of this difference is unclear because Arg5 is involved in crystal packing interactions in both structures. His8 appears to play an indirect role at P_1 (R. Shapiro, unpublished results). In D116H, His8 is ∼2 Å closer to P_1 than it is in Ang, but this residue, like Arg5, participates in crystal contacts that might influence its position.

[2] The active sites of RNase A and its homologues contain subsites, designated P_0−P_n, B_0−B_n, and R_0−R_n (*1*, *2*), for binding the phosphate, nucleobase, and ribose moieties of RNA substrates, respectively. The core dinucleotide occupies the B_1, R_1, P_1, B_2, and R_2 subsites.

Table 4: Potential Hydrogen Bonds in the Ribonucleolytic Active Site of Human Ang and Its D116H, Q117G, I119A/F120A, and Des(121−123) Variants[a]

donor	acceptor	wild-type	D116H	Q117G	I119A/F120A	des(121−123)
His8 Nϵ2	Gln12 Oϵ1	2.9	3.3	−	3.3	2.9
His13 Nδ1	Thr44 O	2.9	2.9	3.0	3.1	2.7
His13 Nϵ2	water	3.0	−	3.1	2.9	3.0
Lys40 Nζ	Asn43 Oδ1	−	−	2.8	2.9	2.8
Lys40 Nζ	Ile41 O	−	−	−	−	2.9
Lys40 Nζ	Gln117 Oϵ1 (B)[b]	−	−	−	−	2.9
Thr44 N	Gln117 Oϵ1	2.9	3.0	−	2.8	2.6
Thr44 N	water	−	−	3.0	−	−
Thr44 Oγ1	Thr80 Oγ1	2.8	3.1	2.8	2.7	2.9
Lys82 Nζ	Phe120 OT2	−	−	−	−	3.1
Arg101 Nη1	Ile119 O	−	3.2	−	−	−
Arg101 Nη1	Ala119 O	−	−	−	3.0	−
His114 Nδ1	water	2.8	−	3.1	−	2.7
His114 Nϵ2	water	2.8	2.8	2.7	2.5	2.7
His116 Nδ1	water	−	2.3	−	−	−
Gln117 Nϵ2	Thr44 Oγ1	3.1	2.9	−	2.7	2.6
Gln117 Oϵ1 (B)[b]	Ile42 O	−	−	−	−	2.8
Gln117 Nϵ2 (B)[b]	water	−	−	−	−	3.3
Gln117 N	Leu115 O	−	2.6	−	2.8	−
Gln117 N	water	−	−	−	−	3.0
Gly117 N	Leu115 O	−	−	3.2	−	−
Ser118 N	Asp116 Oδ1	3.1	−	2.9	−	3.2
Ser118 Oγ	Asp116 Oδ1	2.5	−	2.6	3.0	3.0
Phe120 N	Gln117 O	3.0	−	−	−	3.1
Phe120 N	Gly117 O	−	−	3.0	−	−
Arg121 N	Ser118 O	3.1	2.9	3.3	−	−
Arg121 Nη1	Asp41 Oδ1	−	3.0	−	−	−
water	Gln12 Oϵ1	−	−	3.3	2.7	2.9
water	Thr44 Oγ1	−	−	2.8	−	−
water	Asp116 Oδ2	2.9	−	3.1	2.4	−
water	Ile119 O	2.8	−	2.7	−	−
water	Phe120 O	3.0	−	3.1	−	−

[a] Values are distances in angstroms. Hydrogen bonds are listed if the distance between a donor (D) and an acceptor (A) is shorter than 3.3 Å and if the D−H−A angle is greater than 120°. Hydrogen bond parameters were calculated with the program HBPLUS (*71*). [b] B denotes an alternative conformation of Gln117 seen only in the des(121−123) structure (see the text).

Replacement of Asp116 with His amplifies angiogenic potency as well as ribonucleolytic activity (*32*). Although it is possible that the increased biological activity is simply a consequence of the enhancement in catalytic efficiency, it is also conceivable that it derives from improvements in the binding of Ang to endothelial cells or its subsequent nuclear translocation, both of which are critical for induction of neovascularization. These cellular interactions are known to involve, minimally, residues of the segments of positions 60−68 and 108−111 (cell binding) and 31−33 (translocation) (*62*−*64*). In D116H, His116 forms van der Waals contacts with Leu69 that are not made by Asp116 in wild-type Ang that might have some impact on cell binding. However, the main chains of the cell-binding elements in D116H and Ang superimpose well (Figure 5), and only the side chain of Asn68 (which is relatively flexible in the structures) diverges appreciably. The nuclear translocation element also corresponds closely in the two structures, with the exception of the side chain of Arg31, which is involved in crystal contacts in D116H.

Structure of Q117G. Gln117 corresponds to Ala122 of RNase A, the side chain of which travels away from the active site. Therefore, this residue was not suspected to be functionally important prior to the determination of the Ang crystal structure. The obstructive location of Gln117 revealed by the structure reflects the markedly different secondary structure of the C-terminal segment in Ang (*28*); residue 122 in RNase A extends β-strand 7, whereas residue 117 in Ang initiates a short 3_{10} helix. The helical turn places the side chain of Gln117 within the putative B_1 binding pocket, where its carboxyamido group forms hydrogen bonds with the side chain hydroxyl and main chain N of Thr44 that mimic those made by pyrimidines in nucleotide complexes of RNase A (*65*−*67*) (Figure 2A).

Superposition of the Ang structure with those of the RNase A complexes shows that the main chain atoms of residue 117 lie within 1−2.5 Å of the N3, C4, and C5 atoms of the pyrimidine, and hence are also obstructive. Thus, removal of the side chain, by itself, should not be sufficient to provide access to the B_1 site. Nonetheless, replacement of Gln117 with Gly increases the ribonucleolytic activity of Ang by 21−30-fold (*34*). This enhancement could have at least three sources. (i) The loss of the hydrogen bonds between residues 117 and 44 might cause the free protein to adopt the same, as yet undefined, B_1 open conformation that forms during the normal catalytic pathway of wild-type Ang. (ii) The loss of these hydrogen bonds might lower the energetic cost of the conformational change, but not induce it. (iii) The removal of the side chain might allow a different, less extensive conformational change that moves the main chain of residue 117 the few angstroms necessary to open the pyrimidine site.

The crystal structure of Q117G, determined at 1.8 Å resolution, shows that the first of these explanations does not apply; i.e., the variant structure is essentially identical to that of Ang except for the loss of the side chain of residue 117. The conformation of the segment of residues 114−121 is not altered by the replacement (Figure 6), and all of the

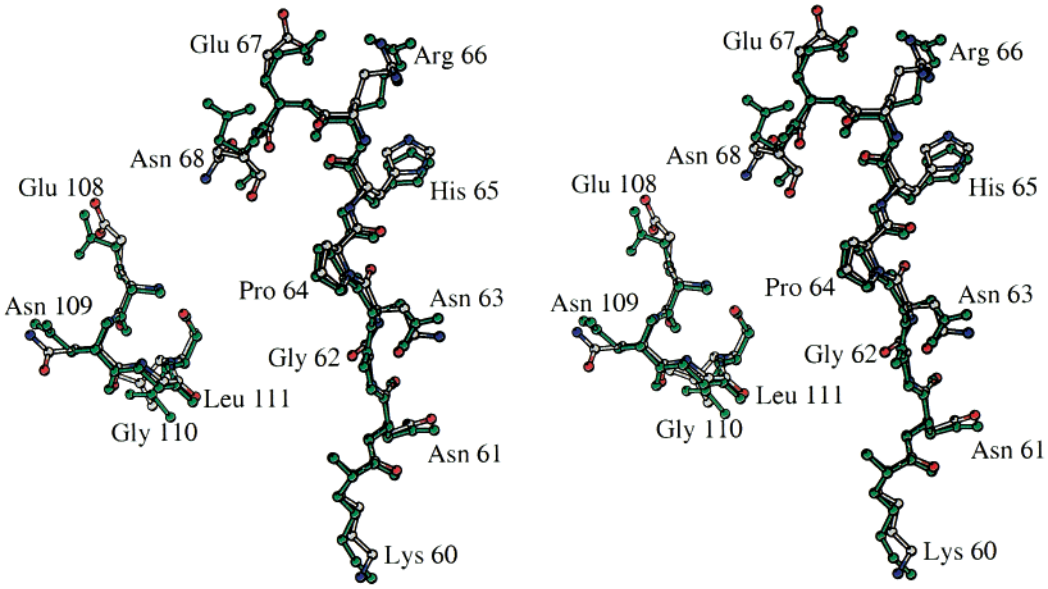

FIGURE 5: Stereoview of the superimposed structures of wild-type Ang (green) and D116H (standard coloring scheme) showing residues 60−68 and 108−111 in the putative cell binding site.

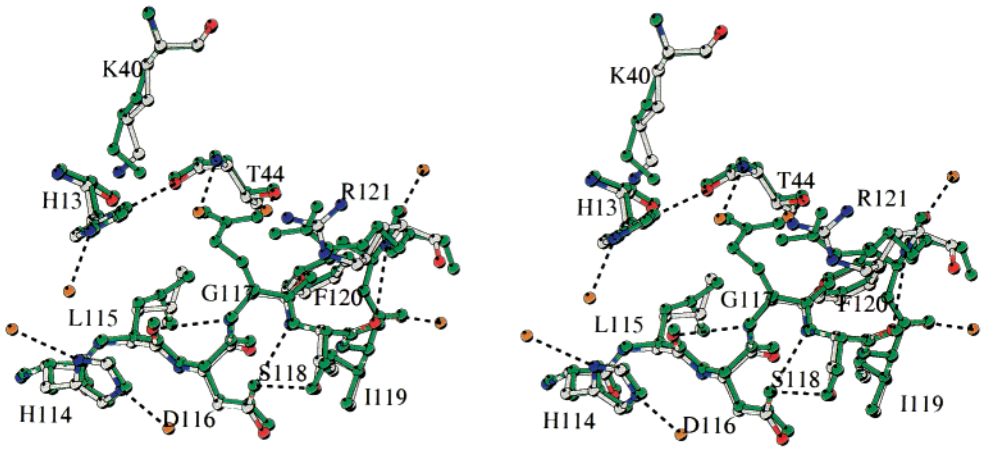

FIGURE 6: Stereoview of the superimposed structures of wild-type Ang (green) and Q117G (standard coloring scheme) as in Figure 4.

hydrogen bonds (Table 4) and hydrophobic contacts of segment residues other than residue 117 are retained. The main chain atoms of residue 117 have moved by 0.3−0.4 Å, an amount well below that required to open the B_1 site. However, it is possible that such a minor localized movement of the main chain of residue 117 occurs in the presence of ligand, and that this accounts for the increased activity of Q117G (see Conclusions). The orientations of the catalytic residues are unchanged, except that Nζ of Lys40 diverges by 1.1 Å from its location in wild-type Ang. Two water molecules, both with low temperature factors, occupy positions close to those of Oϵ1 and Nϵ2 of residue 117 in the native structure and make analogous hydrogen bonds with Thr44 (Table 4 and Figure 6).

Structure of I119A/F120A. Ile119 and Phe120 of human Ang are conserved or replaced with other hydrophobic residues in bovine, mouse, rabbit, and pig Ang (*68*−*70*). In the human Ang crystal structure, the side chains of these residues are largely buried [accessible surface areas are 25 (Ile119) and 4 Å^2 (Phe120)] in a region that contains components from five β-strands: β1 (Thr44), β4 (Val78 and Thr80), β5 (Arg101), β6 (Val103, Val104, and Val105), and β7 (Leu115); Ile119 and Phe120 form six van der Waals contacts with each other and 10 with additional amino acids (Figure 2B). These observations suggest that hydrophobic interactions of Ile119 and Phe120 might help to orient the C-terminal segment and thereby contribute to placement of Gln117 within the B_1 site (*33*). Moreover, the side chain of Phe120 itself intrudes into the putative B_1 pocket; the Cγ and Cδ2 atoms of this residue lie less than 2 Å from the site where O4 or N4 of substrate pyrimidines is expected to bind (*22*).

Simultaneous replacements of Ile119 and Phe120 with Ala increase enzymatic activity by 3−4-fold (*33*), demonstrating that these residues indeed have a suppressive role. A similar degree of activation is observed when the catalytic efficiency of wild-type Ang is measured in the presence of 45% methanol, which might be expected to weaken or eliminate the hydrophobic interactions of Ile119 and Phe120. In contrast, the potency of I119A/F120A is barely affected by methanol. Thus, the activation of Ang by methanol appears to involve Ile119 and Phe120, consistent with the view that the hydrophobic burial of these residues stabilizes the inactive conformation of Ang.

The crystal structure of I119A/F120A, determined at 2.3 Å resolution, reveals only modest changes in the positions

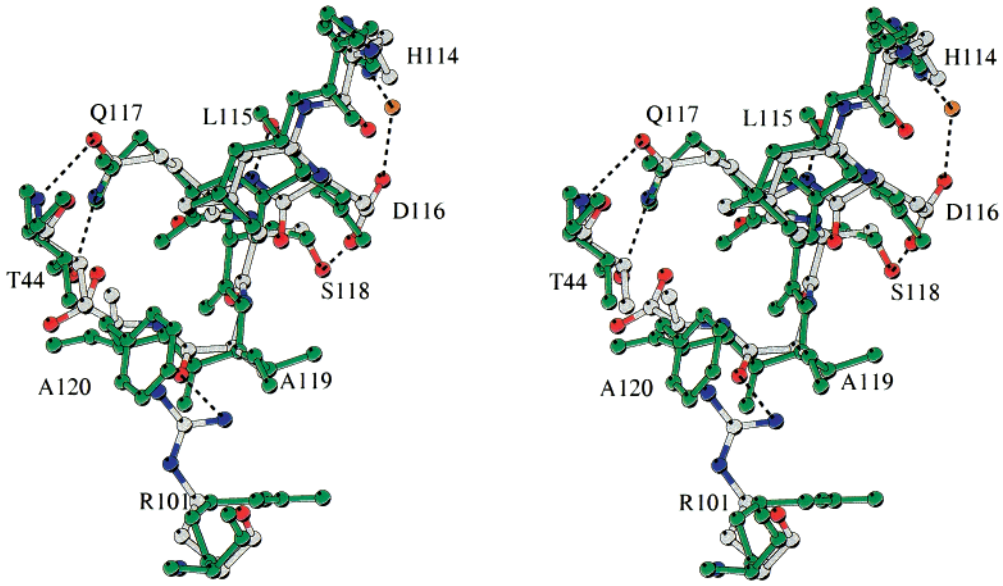

FIGURE 7: Stereoview of the superimposed structures of wild-type Ang (green) and I119A/F120A (standard coloring scheme) as in Figures 4 and 6, but rotated to highlight the positions of the amino acid replacements.

of the C-terminal residues, and Gln117 continues to block the putative B_1 site (Figure 7). However, the mobility of this segment is dramatically increased. As noted above, there is no electron density for residues 121−123 and the density for residues 119 and 120 is very weak. In addition, the temperature factors for all atoms of Ser118 are extremely high (67−82 vs 20−25 Å^2 in wild-type Ang) and those for Gln117 are significantly higher in the variant (41−59 Å^2) than in the wild-type protein (19−22 Å^2), whereas the averages for all protein atoms in the two structures are nearly identical (30 vs 31 Å^2). The Asp116 carboxylate is also somewhat more flexible in the I119A/F120A structure. As a consequence of the general loosening of the C-terminal segment, residues 117−121 no longer form a 3_{10} helix (Table 4). The hydrogen bond between Oδ1 of Asp116 and N of Ser118 is absent as well, and Oδ2 of Asp116 now forms a water-mediated hydrogen bond with Nϵ2 of His114, like that made by His116 of D116H. Although Oδ1 of Asp116 is still positioned to hydrogen bond with the main chain N of Ser118, the high mobility of the latter residue indicates that in fact there is no strong interaction. Similar considerations apply to the two hydrogen bonds of Gln117 Oϵ1 and Nϵ2 with N and Oγ1 of Thr44, respectively; the distances and angles are similar to those in wild-type Ang, but the greater flexibility of the side chain of residue 117 in I119A/F120A suggests that these interactions are less stable. The space occupied by the Phe120 phenyl group in Ang is now partially filled by the Arg101 guanidino group, which has moved 4−5 Å and hydrogen bonds with the main chain oxygen of Ala119.

The conformations of the other residues in the active site region are largely unaffected by the double replacement. Arg5, Gln12, His13, Thr44, Glu108, and His114 are all within 0.5 Å of their positions in wild-type Ang. Lys41 diverges at Nζ as in the Q117G structure. His8 is shifted somewhat, but still forms a hydrogen bond with Gln12.

Structure of Des(121−123). Arg121, Arg122, and Pro123 of human Ang are neither conserved nor conservatively substituted in the angiogenins of the other species examined to date. Nonetheless, the proximity of these residues to the active site and to residues 116−120 raises the possibility that they might have some functional role. Moreover, Arg121, as the final residue of the 3_{10} helix, forms a main chain hydrogen bond with Ser118 that appears to stabilize the inactive conformation. The importance of these amino acids was investigated by producing the deletion mutant des-(121−123) (*33*). The enzymatic activity of the variant toward dinucleotide substrates was found to be nearly the same as that of the wild-type protein (Table 1), whereas potency with tRNA and poly(C) was reduced by 10-fold. On this basis, Russo et al. (*33*) proposed that residues 121−123 play a positive role in cleavage of polynucleotides by participating in a peripheral substrate binding subsite beyond the core region of the B_1, P_1, and B_2 sites.

Examination of the crystal structure of des(121−123), determined at 1.8 Å resolution, reveals a potential alternative explanation for the decreased enzymatic activity of this variant toward large substrates; Lys82, which had been considered to be a possible B_0 site residue on the basis of modeling (*61*), adopts a position markedly different from that seen in the wild-type Ang structure (Figure 8). The Nζ atom of this residue is 7.4 Å away from its location in Ang, and forms a hydrogen bond with the Phe120 C-terminal α-carboxylate (Table 4). If Lys82 indeed serves as part of the B_0 site, it is unlikely to fulfill this function from its altered location. Thus, the effect of the deletion of residues 121−123 on activity might be due to the movement of Lys82 rather than to the loss of any direct interactions of the C-terminal tripeptide with substrate. Although Lys82 is also shifted considerably in the crystal structures of D116H and I119A/F120A, it is poorly defined in these other structures [whereas it is well-defined in des(121−123)] and does not form any interactions that might fix its position. Asp41, another proposed B_0 residue, has also moved in the des-(121−123) structure, but in this case, the altered positioning may reflect an interaction of the β-carboxylate with the bound citrate molecule.

The residues in the C-terminal segment and active site region of des(121−123) are positioned essentially as in wild-type Ang (Figure 8) and form largely the same set of

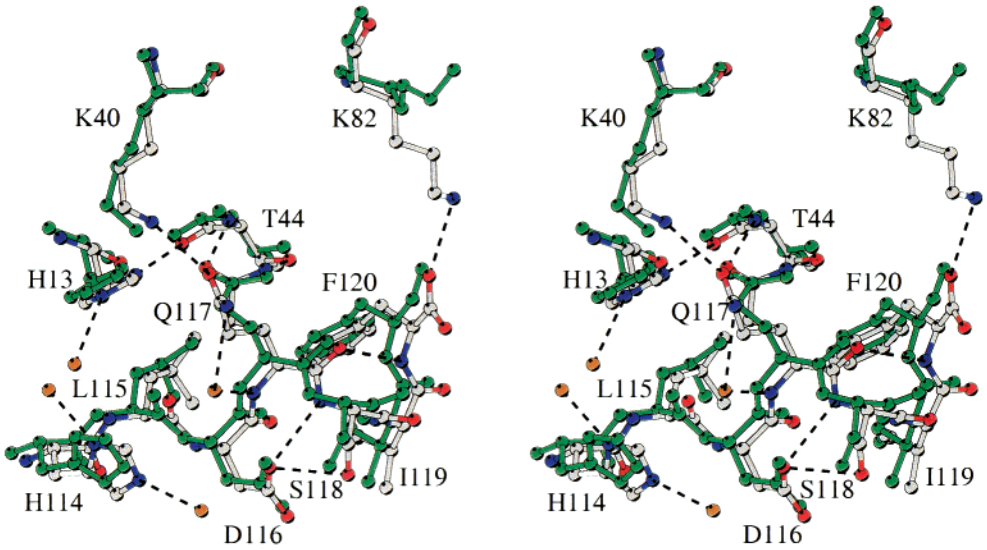

FIGURE 8: Stereoview of the superimposed structures of wild-type Ang (green) and des(121−123) (standard coloring scheme) as in Figures 4 and 6, except that Lys82 has been added.

hydrogen bond (Table 4) and van der Waals interactions. However, Gln117 adopts two alternative conformations that are related by a 60° rotation around the $C_\gamma-C_\delta$ axis. One of these conformations corresponds to that in wild-type Ang. The other also obstructs the B_1 subsite, although in this case the carboxyamido group of residue 117 lies closer to the position where N1 and C1′ (rather than O2 and N3) of pyrimidine nucleosides are expected to bind. The interactions with Thr44 are lost, and Gln117 Oϵ1 makes a hydrogen bond with Nζ of Lys40 instead.

Conclusions. The results of molecular modeling strongly suggest that the native conformation of Ang is inactive and that a major structural rearrangement of the C-terminal region to open the B_1 site is required for Ang to cleave RNA (*34*). Changes in substrate, rather than enzyme, conformation, e.g., rotations around the glycosidic bond or modifications of the ribose pucker of the pyrimidine nucleotide, do not appear to be capable of alleviating the blockage. Further support for the existence of the proposed restructuring is provided by the marked changes in activity and C versus U preference that occur when Thr44 is mutated (*21*); these effects indicate that Thr44 interacts directly with pyrimidines, which it cannot do unless Gln117 moves at least several angstroms from its observed position(s).

The closed conformation observed in the Ang crystal structure appears to be stabilized by a combination of hydrogen bonds and hydrophobic interactions. The two hydrogen bonds of Gln117 with Thr44 seem to "pull" Gln117 into the B_1 site and anchor it there, while the hydrogen bonds of Asp116 with Ser118 and those generating the helix of residues 117−121, together with the hydrophobic burial of the Ile119 and Phe120 side chains, define the orientation of the main chain to "push" Gln117 into the B_1 site. From this vantage point, it is reasonable that replacements of Asp116, Gln117, Ile119, and Phe120 would all destabilize the closed conformation and thereby increase enzymatic potency. However, the crystal structures of the D116H, Q117G, and I119A/F120A variants presented here, together with analysis of the functional effects of the mutations, indicate that the basis for activation may be more complex.

Strikingly, in all three variant structures, the enzyme continues to adopt the closed conformation, demonstrating that no individual residue among those mutated, by itself, is critical for maintaining this conformation. The Q117G crystal structure differs from that of wild-type Ang with respect to only residue 117, whereas those of D116H and I119A/F120A show significant perturbations of the C-terminal region beyond the replacement site. In D116H, the residues in the segment of residues 117−121 have lost their helicity and undergone a partial reorientation. In I119A/F120A, the entire C-terminal region has become much more mobile and all of the hydrogen bonds thought to stabilize the obstructive conformation have been lost or weakened (as indicated by the high temperature factors of the atoms that are involved). These observations suggest that in fact the hydrogen bonds of Gln117 with Thr44 may be less important than the interactions of residues 116, 119, and 120 for maintaining the native conformation. Indeed, Lequin et al. (*29*, *31*) had concluded from the NMR structures of human and bovine Ang that the hydrogen bonds between residues 117 and 44 (residues 118 and 45 in bovine Ang) are transient; the side chain of residue 117 (or 118) occupies multiple positions, and the Thr44 (or Thr45) amide and hydroxylic protons are not protected. The des(121−123) crystal structure also shows the carboxyamide of residue 117 in an alternative (although still obstructive) orientation.

If (i) the B_1 site is still blocked in Q117G and (ii) the hydrogen bonds between residues 117 and 44 are weak (and thus their removal would not shift the closed−open equilibrium appreciably), then why is Q117G 30-fold more active than wild-type Ang? This activation is perhaps most easily understood if the "open conformation" that is reached during the Q117G-catalyzed reaction involves only a localized movement of the main chain of residue 117 out of the B_1 site, rather than the more elaborate reorientation that occurs with the wild-type enzyme. In this scenario, other functional aspects of the Gln117 replacements can also be rationalized. For example, the ~2-fold greater activity of Q117G as compared to that of Q117A (*34*) might reflect the lesser difficulty of pushing Gly rather than Ala out of the B_1 site.

Moreover, the availability of a localized minor conformational adjustment for Q117G might also account for the nonadditivity of the effects of Gln117 and Asp116 replacements (*34*), if the Asp116 variant follows the wild-type reorientation and the double variant primarily undergoes the more limited change. A previous hypothesis, which the crystal structures of Q117G and D116H now demonstrate to be false, was that the mutational effects are not additive because each substitution alone is sufficient to open the B_1 site.

In some respects, D116H appears to be a more straightforward case than Q117G. The crystal structure shows that both of the stabilizing hydrogen bonds between residues 116 and 118 have been lost, and that the C-terminal secondary structure has partially melted, as might be expected from such destabilization. Moreover, the 7-fold activation that results from replacement of Ser118 with Ala (*35*) provides independent evidence (lacking for residues 117 and 44; see ref *21*) that at least one of the hydrogen bonds between residues 116 and 118 is moderately strong. At the same time, the simple attribution of the activity increase to facilitation of the opening of the B_1 site cannot account for one important facet of D116H; although this variant is 18-fold more active than Ang with polynucleotide substrates, it is activated by only 3-fold with dinucleotide substrates (*32*) (Table 1). This disparity is limited to Asp116 variants (*32*, *36*); that is, substitutions of Gln117, Ser118, Ile119, and Phe120 each increase activity toward large and small substrates in parallel (Table 1 and ref *35*). This type of substrate dependence might arise if replacement of Asp116 (but not the other residues) improves the interactions of the enzyme with peripheral polynucleotide components as well as those with the core dinucleotide. In this case, the extent of activation due to destabilization of the closed conformation might be only the factor of 3 measured with dinucleotide substrates. However, it would then be difficult to understand why substitutions of Ser118, both singly and together with Asp116, produce larger activity increases that are substrate-independent (*35*). Moreover, the D116H crystal structure displays no perturbations that seem likely to influence known peripheral subsites.

The structural basis for the functional changes associated with the Ile119/Phe120 double substitution appears to be still more complex. The crystal structure of I119A/F120A suggests that the closed conformation has been destabilized much more than for D116H and Q117G. Indeed, all of the C-terminal residues starting at residue 117 have become quite mobile, and it is doubtful that any of the strong interactions thought to place Gln117 in the B_1 pocket are still present. Why then is the degree of activation produced by these mutations severalfold smaller than those for replacements of Asp116 and Gln117 (Table 1)? The I119A/F120A structure does contain one new hydrogen bond, connecting Arg101 Nη1 and the main chain O of A119, which might promote the obstruction of the B_1 site. However, the high temperature factors of these atoms (57 and 100 Å^2, respectively) suggest that this bond is weak at best. These observations raise the interesting possibility that interactions other than those already identified may make important contributions to defining the native C-terminal conformation.

In contrast with the other C-terminal variants discussed here, des(121−123) has markedly decreased activity toward polynucleotide substrates. Thus, residues 121−123, unlike residues 116−120, appear to play a largely positive role, originally proposed to involve binding of peripheral substrate components. The crystal structure of des(121−123) supports the view that these residues are not involved in defining the obstructive orientation of the C-terminal segment; the segment of residues 116−120 is entirely well-ordered as in wild-type Ang, and all of the key interactions are maintained. The structure provides no direct evidence for or against the participation of residues 121−123 in binding of large substrates. However, it raises the possibility that movement of a putative peripheral subsite residue, Lys82, rather than the loss of any contacts of residues 121−123 with substrate, might account for the decrease in activity. Interestingly, Lys82 forms a hydrogen bond with the new C-terminus that might be expected to diminish potency by stabilizing the closed conformation. However, in this case, it is unclear why cleavage of small substrates would not be affected similarly.

A more complete understanding of the role of the C-terminal region of Ang must await the determination of the structure of the open conformation that Ang adopts upon binding to substrates and substrate analogues. This has remained elusive because of the relatively low affinity of all known Ang inhibitors, and because in all crystal forms of Ang grown thus far the key B_2 and P_2 binding subsites are occupied by residues from neighboring molecules (see ref *60*). It seems likely that the structure of the active conformation will reveal additional, perhaps positive, roles for some of the residues whose contributions have been demonstrated to be negative. For example, in the active conformation, Asp116 might help orient His114 for catalysis, as does Asp121 (with His119) in RNase A. The activity increases observed in these instances would then reflect the net difference between the effects of losing activity-suppressing and activity-enhancing interactions.

ACKNOWLEDGMENT

We are grateful to the staff at the Synchrotron Radiation Source at Daresbury, England, for help with X-ray data collection.

REFERENCES

1. Richards, F. M., and Wyckoff, H. W. (1971) *Enzymes 4*, 647−806.
2. Pares, X., Nogues, M. V., de Llorens, R., and Cuchillo, C. M. (1991) *Essays Biochem. 26*, 89−103.
3. Riordan, J. F. (1997) in *Ribonucleases: Structures and Functions* (D'Alessio, G., and Riordan, J. F., Eds.) pp 445−489, Academic Press, New York.
4. Adams, S. A., and Subramanian, V. (1999) *Angiogenesis 3*, 189−199.
5. Fett, J. W., Strydom, D. J., Lobb, R. R., Alderman, E. M., Bethune, J. L., Riordan, J. F., and Vallee, B. L. (1985) *Biochemistry 24*, 5480−5486.
6. Olson, K. A., Byers, H. R., Key, M. E., and Fett, J. W. (2001) *Clin. Cancer Res. 7*, 3598−3605.
7. Olson, K. A., Fett, J. W., French, T. C., Key, M. E., and Vallee, B. L. (1995) *Proc. Natl. Acad. Sci. U.S.A. 92*, 442−446.
8. Olson, K. A., French, T. C., Vallee, B. L., and Fett, J. W. (1994) *Cancer Res. 54*, 4576−4579.
9. Piccoli, R., Olson, K. A., Vallee, B. L., and Fett, J. W. (1998) *Proc. Natl. Acad. Sci. U.S.A. 95*, 4579−4583.
10. Chopra, V., Dinh, T. V., and Hannigan, E. V. (1997) *J. Cancer Res. Clin. Oncol. 123*, 167−172.
11. Chopra, V., Dinh, T. V., and Hannigan, E. V. (1998) *Cancer Invest. 16*, 152−159.

12. Hartmann, A., Kunz, M., Kostlin, S., Gillitzer, R., Toksoy, A., Brocker, E. B., and Klein, C. E. (1999) *Cancer Res. 59*, 1578−1583.
13. Etoh, T., Shibuta, K., Barnard, G. F., Kitano, S., and Mori, M. (2000) *Clin. Cancer Res. 6*, 3545−3551.
14. Eberle, K., Oberpichler, A., Trantakis, C., Krupp, W., Knupfer, M., Tschesche, H., and Seifert, V. (2000) *Anticancer Res. 20*, 1679−1684.
15. Bodner-Adler, B., Hefler, L., Bodner, K., Leodolter, S., Frischmuth, K., Kainz, C., and Mayerhofer, K. (2001) *Anticancer Res. 21*, 809−812.
16. Shimoyama, S., and Kaminishi, M. (2000) *J. Cancer Res. Clin. Oncol. 126*, 468−474.
17. Shimoyama, S., Yamasaki, K., Kawahara, M., and Kaminishi, M. (1999) *Clin. Cancer Res. 5*, 1125−1130.
18. Miyake, H., Hara, I., Yamanaka, K., Gohji, K., Arakawa, S., and Kamidono, S. (1999) *Cancer 86*, 316−324.
19. Shapiro, R., Fox, E. A., and Riordan, J. F. (1989) *Biochemistry 28*, 1726−1732.
20. Shapiro, R., and Vallee, B. L. (1989) *Biochemistry 28*, 7401−7408.
21. Curran, T. P., Shapiro, R., and Riordan, J. F. (1993) *Biochemistry 32*, 2307−2313.
22. Leonidas, D. D., Shapiro, R., Allen, S. C., Subbarao, G. V., Veluraja, K., and Acharya, K. R. (1999) *J. Mol. Biol. 285*, 1209−1233.
23. Shapiro, R., Riordan, J. F., and Vallee, B. L. (1986) *Biochemistry 25*, 3527−3532.
24. Shapiro, R., Weremowicz, S., Riordan, J. F., and Vallee, B. L. (1987) *Proc. Natl. Acad. Sci. U.S.A. 84*, 8783−8787.
25. Shapiro, R., Harper, J. W., Fox, E. A., Jansen, H. W., Hein, F., and Uhlmann, E. (1988) *Anal. Biochem. 175*, 450−461.
26. Harper, J. W., and Vallee, B. L. (1989) *Biochemistry 28*, 1875−1884.
27. Strydom, D. J., Fett, J. W., Lobb, R. R., Alderman, E. M., Bethune, J. L., Riordan, J. F., and Vallee, B. L. (1985) *Biochemistry 24*, 5486−5494.
28. Acharya, K. R., Shapiro, R., Allen, S. C., Riordan, J. F., and Vallee, B. L. (1994) *Proc. Natl. Acad. Sci. U.S.A. 91*, 2915−2919.
29. Lequin, O., Thuring, H., Robin, M., and Lallemand, J. Y. (1997) *Eur. J. Biochem. 250*, 712−726.
30. Acharya, K. R., Shapiro, R., Riordan, J. F., and Vallee, B. L. (1995) *Proc. Natl. Acad. Sci. U.S.A. 92*, 2949−2953.
31. Lequin, O., Albaret, C., Bontems, F., Spik, G., and Lallemand, J. Y. (1996) *Biochemistry 35*, 8870−8880.
32. Harper, J. W., and Vallee, B. L. (1988) *Proc. Natl. Acad. Sci. U.S.A. 85*, 7139−7143.
33. Russo, N., Nobile, V., Di Donato, A., Riordan, J. F., and Vallee, B. L. (1996) *Proc. Natl. Acad. Sci. U.S.A. 93*, 3243−3247.
34. Russo, N., Shapiro, R., Acharya, K. R., Riordan, J. F., and Vallee, B. L. (1994) *Proc. Natl. Acad. Sci. U.S.A. 91*, 2920−2924.
35. Shapiro, R. (1998) *Biochemistry 37*, 6847−6856.
36. Curran, T. P., Shapiro, R., Riordan, J. F., and Vallee, B. L. (1993) *Biochim. Biophys. Acta 1202*, 281−286.
37. Shapiro, R., and Vallee, B. L. (1992) *Biochemistry 31*, 12477−12485.
38. Acharya, K. R., Subramanian, V., Shapiro, R., Riordan, J. F., and Vallee, B. L. (1992) *J. Mol. Biol. 228*, 1269−1270.
39. Kabsch, W. (1988) *J. Appl. Crystallogr. 21*, 916−924.
40. Otwinowski, Z., and Minor, W. (1997) *Methods Enzymol. 276*, 307−326.
41. Collaborative Computational Project No. 4 (1994) *Acta Crystallogr. D50*, 760−763.
42. French, S., and Wilson, K. (1978) *Acta Crystallogr. A34*, 517−525.
43. Navaza, J. (1994) *Acta Crystallogr. A50*, 157−163.
44. Brünger, A. T., Kuriyan, J., and Karplus, M. (1987) *Science 235*, 458−460.
45. Jones, T. A., Zou, J.-Y., Cowan, S. W., and Kjeldgaard, M. (1991) *Acta Crystallogr. A47*, 110−119.
46. Read, R. J. (1986) *Acta Crystallogr. A42*, 140−149.
47. Cowtan, K. (1994) *Joint CCP4 and ESF-EACBM Newsletter on Protein Crystallography 31*, 34−38.
48. Brünger, A. T. (1992) *Nature 355*, 472−475.
49. Jiang, J. S., and Brünger, A. T. (1994) *J. Mol. Biol. 243*, 100−115.
50. Laskowski, R. A., MacArthur, M. W., Moss, D. S., and Thornton, J. M. (1993) *J. Appl. Crystallogr. 26*, 283−291.
51. Stuart, D. I., Levine, M., Muirhead, H., and Stammers, D. K. (1979) *J. Mol. Biol. 134*, 109−142.
52. Kraulis, P. J. (1991) *J. Appl. Crystallogr. 24*, 946−950.
53. Esnouf, R. M. (1997) *J. Mol. Graphics Modell. 15*, 132−134.
54. Beintema, J. J., Schuller, C., Irie, M., and Carsana, A. (1988) *Prog. Biophys. Mol. Biol. 51*, 165−192.
55. Stern, M. S., and Doscher, M. S. (1984) *FEBS Lett. 171*, 253−256.
56. Wodak, S. Y. (1977) *J. Mol. Biol. 116*, 855−875.
57. Campbell, R. L., and Petsko, G. A. (1987) *Biochemistry 26*, 8579−8584.
58. Wlodawer, A., Svensson, L. A., Sjolin, L., and Gilliland, G. L. (1988) *Biochemistry 27*, 2705−2717.
59. Schultz, L. W., Quirk, D. J., and Raines, R. T. (1998) *Biochemistry 37*, 8886−8898.
60. Leonidas, D. D., Chavali, G. B., Jardine, A. M., Li, S., Shapiro, R., and Acharya, K. R. (2001) *Protein Sci. 10*, 1669−1676.
61. Russo, N., Acharya, K. R., Vallee, B. L., and Shapiro, R. (1996) *Proc. Natl. Acad. Sci. U.S.A. 93*, 804−808.
62. Hallahan, T. W., Shapiro, R., Strydom, D. J., and Vallee, B. L. (1992) *Biochemistry 31*, 8022−8029.
63. Hallahan, T. W., Shapiro, R., and Vallee, B. L. (1991) *Proc. Natl. Acad. Sci. U.S.A. 88*, 2222−2226.
64. Moroianu, J., and Riordan, J. F. (1994) *Biochem. Biophys. Res. Commun. 203*, 1765−1772.
65. Borah, B., Chen, C. W., Egan, W., Miller, M., Wlodawer, A., and Cohen, J. S. (1985) *Biochemistry 24*, 2058−2067.
66. Richards, F. M., and Wyckoff, H. W. (1973) in *The Atlas of Molecular Structures in Biology* (Phillips, D. C., and Richards, F. M., Eds.) Clarendon Press, Oxford, England.
67. Zegers, I., Maes, D., Dao-Thi, M. H., Poortmans, F., Palmer, R., and Wyns, L. (1994) *Protein Sci. 3*, 2322−2339.
68. Maes, P., Damart, D., Rommens, C., Montreuil, J., Spik, G., and Tartar, A. (1988) *FEBS Lett. 241*, 41−45.
69. Bond, M. D., Strydom, D. J., and Vallee, B. L. (1993) *Biochim. Biophys. Acta 1162*, 177−186.
70. Bond, M. D., and Vallee, B. L. (1990) *Biochem. Biophys. Res. Commun. 171*, 988−995.
71. McDonald, I. K., and Thornton, J. M. (1994) *J. Mol. Biol. 238*, 777−793.
72. Nicholls, A., and Honig, B. (1991) *J. Comput. Chem. 12*, 435−445.

BI015768Q